

Electrically Tunable Printed Bifocal Liquid Crystal Microlens Arrays

Waqas Kamal,* Jia-De Lin, Steve J. Elston, Taimoor Ali, Alfonso A. Castrejón-Pita,* and Stephen M. Morris*

In this communication, the fabrication of electrically tunable bifocal liquid crystal (LC) microlenses using drop-on-demand inkjet printing is demonstrated. By treating the glass substrate with a homeotropic alignment layer, the printed droplets are found to form plano-convex lenses with focal lengths in the range of 220–463 μm , depending upon the number of droplets deposited at each location on the substrate. The precision of the process allows for the microlenses to be deposited in between in-plane indium tin oxide electrodes. In the presence of a high amplitude electric field, the director within the LC droplets is observed to align with the direction of the applied field, but without any accompanying distortion in the droplet profile. However, these changes in the LC director alignment are found to result in a bifocal behavior rather than a continuous change in the focal length. It is also found that there exists a range of voltages for which two focal planes are observed.

Microlenses are of technological importance for a range of applications, such as photovoltaics, solar concentrators, imaging, sensing, beam-steering, and optical interconnects.^[1–11] In recent years inkjet printing is rapidly becoming an attractive method for fabricating microlenses^[12] as it enables the scalable deposition of multiple materials on a variety of substrates with high precision and is an economical process for fabricating microlens arrays over large areas. For example, with this method droplets can be ejected rapidly so that it is possible to build up large arrays of 1000s of microlenses in a matter of seconds. Tunability of the focal length adds functionality to the microlenses^[13–21] and it has recently been reported that drop-on-demand (DoD) inkjet printing can be employed to

fabricate thermally tunable liquid crystal (LC) microlenses.^[22] Printed LC microlens arrays are particularly appealing for the development of switchable 2D/3D autostereoscopic organic light emitting diode (OLED) displays as the printing process ensures that the lenses could be deposited directly onto the pixelated OLED layer without the need for additional glass substrates, which would increase fabrication complexity and device thickness.^[23–25]

In ref. [22], it was demonstrated that, by either increasing or decreasing the temperature, the focal lengths of the printed lenses could be tuned due to an order parameter-induced change in the refractive indices. The reliance on thermal tuning is, however, rather limiting and would not be

practical for the applications described above. While the printing process allows for the rapid fabrication of large arrays of microlenses in short timescales it needs to be combined with a voltage tunable focal length to make use of the switchable nature of the LCs and to ensure that it could be used in applications, such as switchable 2D/3D autostereoscopic OLED displays. Therefore, in this work, we report the development of electrically tunable microlenses and arrays that have been fabricated using DoD deposition onto substrates that consist of in-plane electrodes. **Figure 1** presents illustrations of the electrode configuration as well as photographic images of plano-convex microlenses printed between in-plane electrodes. Figure 1a,b is schematic illustrations of microlenses printed within the 500 μm gap separating two in-plane electrodes and a cross-sectional view of a single microlens with a homeotropic alignment of the director, respectively. The experimental details for printing the microlenses and the processes used to fabricate the in-plane electrode substrates are discussed further in the Experimental Section.

The resulting shape and profile of the LC lenses depends upon the stable ejection of the LC droplet and the surface conditions of the substrate. In this study, a Lecithin-coated substrate, held at 20 °C, was used to promote a plano-convex lens configuration with a homeotropic alignment of the LC director. Surface roughness of the glass substrate can play a role in terms of influencing the droplet configuration and therefore the glass substrates were thoroughly cleaned before the application of the homeotropic alignment layer to remove excess debris. For the glass substrates used in this study, we found that the homeotropic alignment layer was the dominant factor in terms of dictating the resultant droplet profile. Figure 1c shows three high-speed camera images of a single uniform droplet in-flight

W. Kamal, Dr. J.-D. Lin, Prof. S. J. Elston, T. Ali, Dr. A. A. Castrejón-Pita, Dr. S. M. Morris
 Department of Engineering Science
 University of Oxford
 Parks Road, Oxford OX1 3PJ, UK
 E-mail: waqas.kamal@eng.ox.ac.uk;
 alfonso.castrejon-pita@wadham.ox.ac.uk; stephen.morris@eng.ox.ac.uk
 Dr. J.-D. Lin
 Department of Opto-Electronic Engineering
 National Dong Hwa University
 Hualien 974, Taiwan

 The ORCID identification number(s) for the author(s) of this article can be found under <https://doi.org/10.1002/admi.202000578>.

© 2020 The Authors. Published by WILEY-VCH Verlag GmbH & Co. KGaA, Weinheim. This is an open access article under the terms of the Creative Commons Attribution License, which permits use, distribution and reproduction in any medium, provided the original work is properly cited.

DOI: 10.1002/admi.202000578

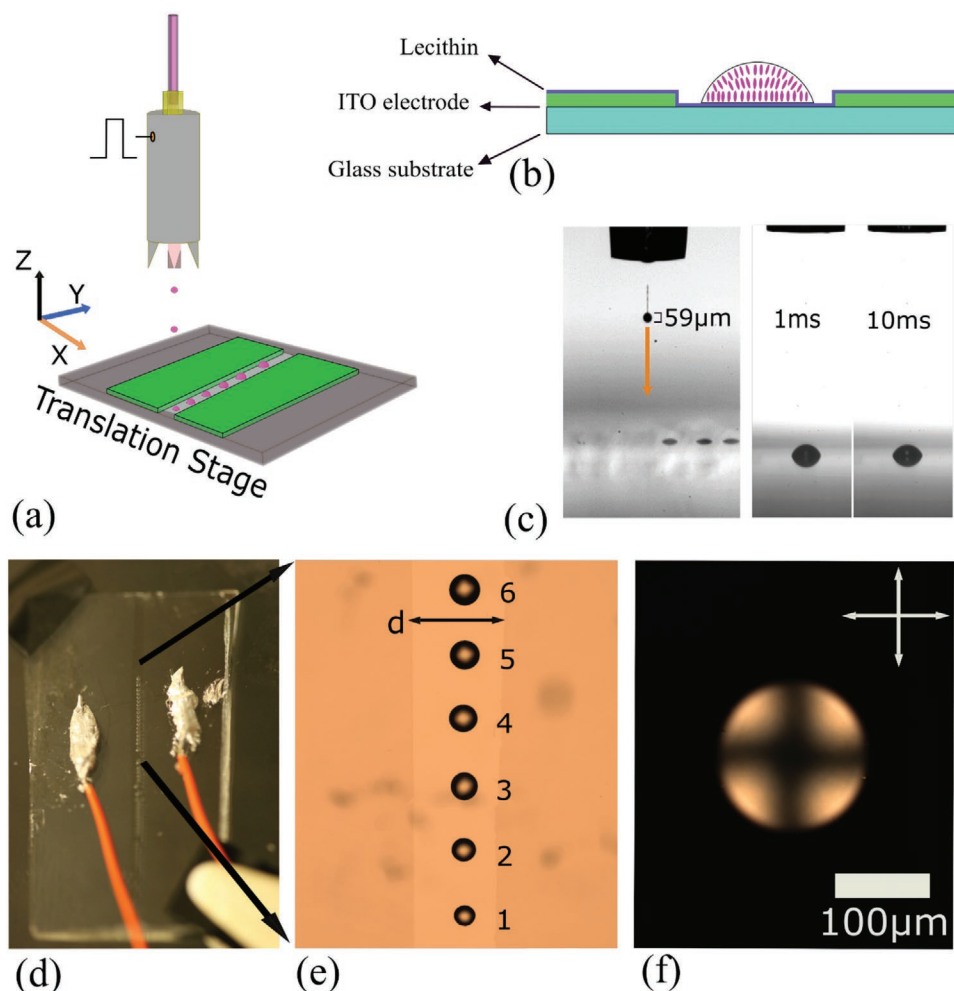


Figure 1. a) Illustration of the process for fabricating microlens arrays using DoD inkjet printing. b) Illustration of a cross-section of a glass substrate with in-plane electrodes and a single printed microlens showing the orientation of the LC director. c) High speed camera images showing the ejection of an LC droplet before and after impact with the substrate. d) Photograph showing an array of microlenses printed on an in-plane electrode substrate. e) Optical microscope image (uncrossed polarizers) of microlenses with different droplet diameters. The numbers indicate the number of drops deposited at each location. f) Crossed polarizer optical microscopy image of a single microlens. The white arrows indicate the orientation of the transmission axes of the polarizers. Both images (e) and (f) were taken on a BX51 Olympus microscope with a halogen white light source.

as well as images at 1 and 10 ms after deposition onto substrate. During flight, the droplet was found to have a diameter of $59 \pm 5 \mu\text{m}$ (slightly larger than the nozzle size, $50 \pm 1 \mu\text{m}$) and a volume of $108 \pm 20 \text{ pL}$. For a single LC droplet deposited on the substrate it was found to reach equilibrium after $\approx 10 \text{ ms}$, which in this example resulted in a droplet diameter of $120 \mu\text{m}$ at the substrate surface.

To increase the volume of the microlens multiple droplets were landed at the same location on the substrate. Figure 1d,e shows example images of printed microlenses with various diameters between the in-plane, indium-tin-oxide (ITO) electrodes that have been formed using the multiple droplet deposition technique. In contrast to conventional LC lenses, which are typically formed using hole-patterned electrodes, the separation of the gap between the in-plane ITO electrodes in this work does not influence droplet morphology, size, or arrangement as these are defined by the printing process and the surface conditions of the substrate. The ITO coating used was $\approx 100 \text{ nm}$

thick which was insignificant compared to even the smallest diameter lenses ($120 \mu\text{m}$) considered in this study. In addition, all droplets were considerably smaller in diameter than the separation of the electrodes and were therefore sufficiently away from the step edges of the electrodes.

The optical microscopy image in Figure 1e provides a closer inspection of the six inkjet-printed microlenses, with a center-to-center distance chosen to be $100 \mu\text{m}$ to avoid any coalescence between droplets, showing an increase in droplet diameter. All six droplets were produced in a single printing sequence. Figure 1f shows an optical microscope image taken of a microlens between crossed polarizers whereby the dark cross in the image indicates the homeotropic alignment of the LC director. The four bright regions result from birefringence that arises due to the slight tilt in the LC director that is induced by the curvature of the droplet. These findings are in accordance with previous studies.^[22]

Properties, such as the lens diameter and contact angle were determined from calibrated shadowgraphy images. The

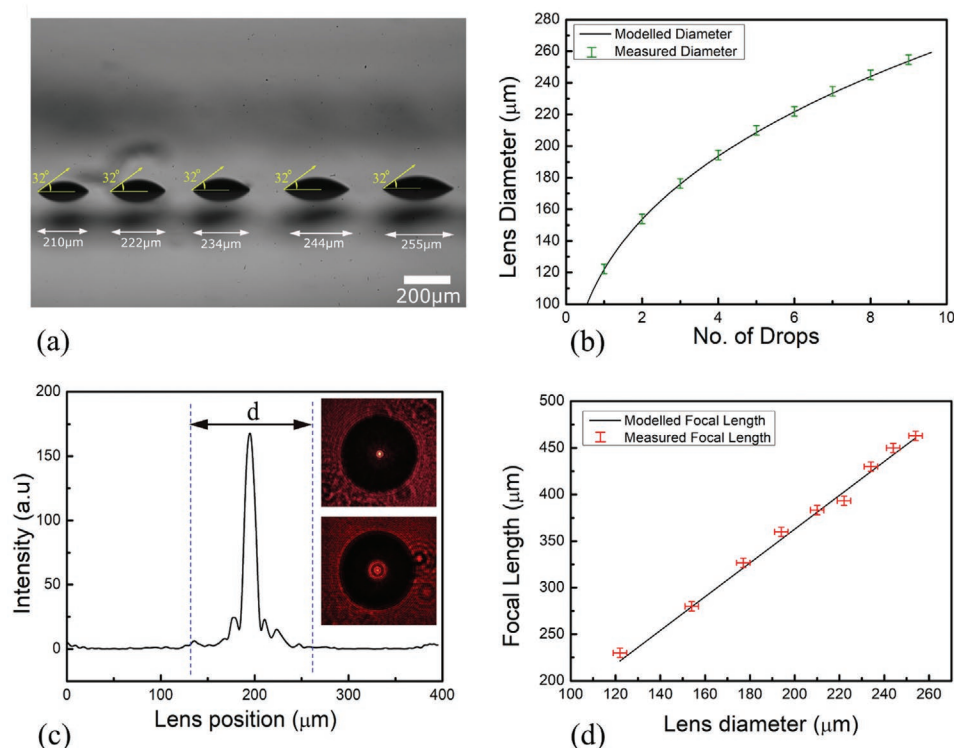


Figure 2. a) Shadowgraphy image of five microlenses with different diameters but with the same contact angle. The same behavior was observed for the smaller droplet diameters considered in this study. b) Lens diameter as a function of the number of drops dispensed by the printer. c) Intensity cross-section of a 255 μm diameter lens at the image plane, along with the CCD images for the in-focus and out-of-focus lens positions (insets). d) Focal length as a function of the microlens diameter.

magnitude of the contact angle, θ , of a printed lens is governed by the balance in the interfacial forces between the glass substrate, the nematic LC, and the surrounding environment.^[26] The contact angle does not, however, depend upon the lens volume, as verified in our measurements of the inkjet-printed lenses, which were all found to be $\theta = 32^\circ \pm 1^\circ$. As an example, shadowgraphy images are presented in Figure 2a for five different droplet diameters ranging from 210 to 255 μm . Identical results were also found for the smaller droplet diameters considered in this study. The relationship between the number of drops and the resulting lens diameter can be seen in Figure 2b, which indicates that the lens diameter is indeed governed by the drop volume and is in good agreement with the modeled drop diameter for a 32° contact angle spherical cap.

The method we have used to characterize the focal length of the LC microlenses follows a method described previously in the literature.^[22,27,28] A schematic of the measurement system is shown in Figure S1 of the Supporting Information (see the Experimental Section for further details). Figure 2c shows the light intensity profile of the focused spot of a 255 μm diameter microlens. The focal length of our plano-convex lenses can be estimated from the Lensmakers' equation, $f = \frac{R}{(n-1)}$ which predicts that the focal length, f , depends only on the radius of curvature, R , and the refractive index, n of the lens. The ordinary refractive index, n_o , of the nematic LC (E7) at 20 $^\circ\text{C}$ and 633 nm is the same for each microlens. As a result, the focal length for the different size microlenses depends only on the radius of curvature, which is emphasized in Figure 2d.

Moreover, the correlation between predictions and experimental results suggests that the small tilt in the LC director due to the curvature of the lens (c.f. Figure 1f) does not significantly affect the focusing properties of the microlenses. This is reasonable because we estimate that the small LC director tilts within the lenses (predominantly near the lens edge) would lead to an elongation in the focal spot of around 15 μm , which is within our measurement accuracy.

To evaluate the tunability of the focal length in the presence of an applied electric field, we first observed the change in the orientation of the LC director on an optical polarizing microscope. Figure 3 presents, as an example, results for a 255 μm diameter microlens, which was chosen due to its low driving voltage as compared to the smaller diameter microlenses, at different applied voltages for a 1 kHz frequency square wave. It is evident from the image sequence that there was no change in the alignment of the LC director from 0 V_{pp} to 100 V_{pp} . However, as the applied voltage exceeded a value of 100 V_{pp} (threshold, V_{th}), a uniformly aligned region started to appear in the center of the microlens which expanded concomitantly with an increase in the applied voltage. By 200 V_{pp} , the uniformly aligned region was found to cover the entirety of the microlens from the center to the periphery of the droplet.

The imaging capability of the 255 μm diameter LC microlens was examined by using a 25 μm grid as an object that was attached to the substrate of the LC microlens. This resulted in a distance between the grid and the LC lens plane of 1.1 mm. In addition, a linear polarizer was positioned just above the

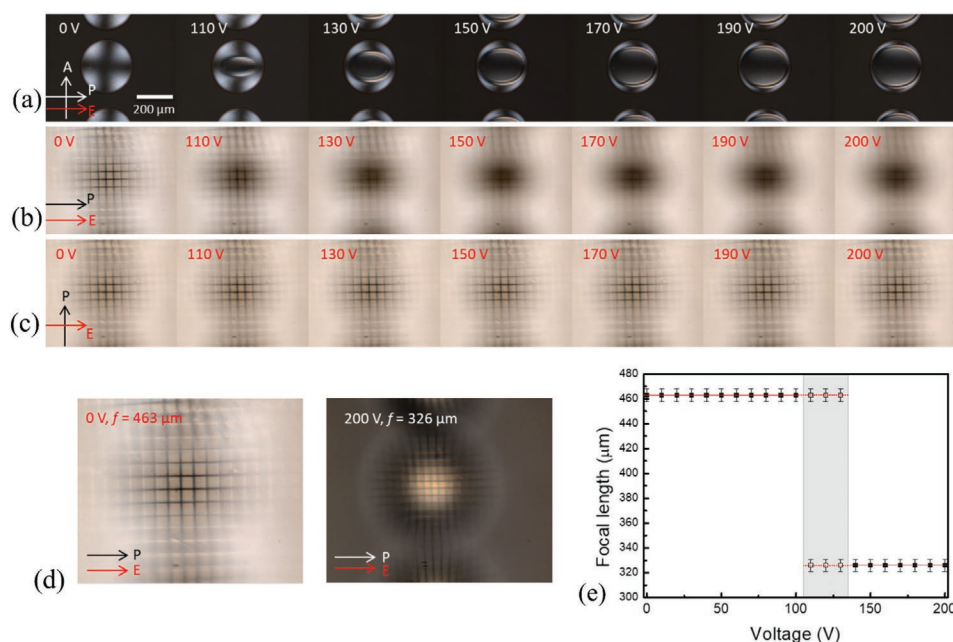


Figure 3. a) Optical polarizing microscopy images of an LC microlens at different applied voltages. Numbers in the top left indicate the peak-to-peak voltage, while the red arrow shows the direction of the applied in-plane electric field and the white arrows show the orientation of the transmission axes of the polarizers. Images of the grid formed by the LC microlens for different applied voltages when the incident polarization is either b) parallel to or c) perpendicular to the direction of the applied in-plane electric field. The black and red arrows represent the orientation of the transmission axis of the polarizer and the direction of the applied in-plane electric field, respectively. The spacing between the lines in the grid is 25 μm. d) Demonstration of the bifocal tunability of the focal length: the image of the grid can be formed at different image planes since the focal length of the LC lens can be either 463 or 326 μm depending on the applied voltage. e) Focal length as a function of the applied voltage for the 255 μm diameter microlens. In this case, the configuration is the same as that shown in (b), i.e., that the direction of the electric field is aligned parallel to the polarization of the incident light. The red lines show the theoretical values of the focal length of the LC lens calculated for a plano convex lens with a refractive index of either $n = 1.52$ (0–130 V_{pp}) or $n = 1.74$ (130–200 V_{pp}).

light source of the microscope so that the input light was linearly polarized. The transmission axis of the polarizer was then adjusted, so that it was parallel to the direction of applied electric field. In this case, for an applied voltage of 200 V_{pp} , the incoming linearly polarized light experiences the extraordinary refractive index of the nematic LC, $n_e = 1.74$ at 20 °C and 633 nm, and therefore a reduced focal length in comparison with the voltage off state. This change in the focal length can be seen in Figure 3b, which shows that when the incident polarization and applied electric field are colinear, the image formed in image plane 1 gradually becomes out of focus (see schematic in Figure S2 for the definition of the image planes, Supporting Information). In contrast, when the incident polarization is aligned perpendicular to the electric field direction, (Figure 3c) the incident light does not experience any change in the refractive index. Therefore, in this case, the focal length will remain the same regardless of the amplitude of the applied electric field.

For voltages from 0 to 100 V the microlenses are polarization insensitive in accordance with the findings in ref. [22]. However, as can be seen in Figure 3b,c, above 100 V the microlenses become polarization sensitive, with focal lengths that differ depending upon whether the polarization is aligned parallel or perpendicular to the direction of the applied electric field. As an example, the left hand image in Figure 3d shows an in-focus image at image plane 1 without the application of an electric field (for the case of the electric field and incident polarization being colinear), whereas the right hand image shows an

in-focus image at the second image plane 2 with a voltage of 200 V_{pp} . The in-focus image at plane 2 was found to be formed at a shorter focal length with reduced magnification, consistent with the larger value of the refractive index. For the case when the polarization is aligned orthogonal to the direction of the applied electric field there is no change in the focal length and the location of image plane, irrespective of the applied voltage.

Quantitative measurements of the focal length of the microlens at various voltages were carried out using the method explained in the Experimental Section (the schematic is presented in Figure S1, Supporting Information) and the results are plotted in Figure 3e. For what follows the incident polarization is aligned along the direction of the applied electric field. At 0 V_{pp} the measured focal length was found to be 463 ± 10 μm. From 0 V_{pp} to 100 V_{pp} no change in the intensity profile, i.e., focal length, was observed. However, for a range of voltages, from 110 V_{pp} to 130 V_{pp} , the LC microlens appeared to exhibit, to some degree, two focal planes. The shaded region in the graph corresponds to the range of voltages for which this behavior was observed, which is also evident in the polarizing microscopy images in Figure 3a. It can be seen that at these voltages the LC director only aligns with the electric field in a small central region. The transition of the LC director from the center to periphery results in regions with different refractive index profiles, which focuses incident light to two separate planes (the image formation of the underlying grid in the Supporting Information S3 shows the duality of the focus).

We believe that the reason for the two focal planes is due to the two separate domains that form in the droplet. As can be seen in Figure 3a, a separate domain is formed within the droplet whereby the director aligns with the electric field direction. This gives rise to a new, shorter focal length. However, between applied voltages of 110 and 130 V the central domain coexists with the outer domain for which the director is aligned orthogonal to the plane of the glass substrates, which corresponds to the smaller refractive index and the longer focal length that exists in the absence of an applied voltage.

From 130 V_{pp} to 200 V_{pp} , the focal length was reduced to a single value of $323 \pm 10 \mu\text{m}$ and remained unchanged with increasing voltage. As seen in Figure 3e, the experimentally measured focal length appears to show bifocal tuning, with only two focal lengths that are accessible using an applied voltage. The droplet boundary and profile was also monitored using shadowgraphy imaging to see whether there was any alteration in the shape of the microlens at the high amplitude voltages. However, no noticeable variation in the microlens profile, through electrowetting, for example, was observed (Figure S4 shows no change in the lens profile, Supporting Information). The change in the focal length is therefore considered to be due solely to a reorientation of the LC director in the presence of an applied electric field. The smaller diameter microlenses as compared to the 255 μm diameter microlens, behaved the same way, however, the driving voltage required to align the LC director was found to be larger. A series of microscope images showing the evolution in the director alignment of the 222 μm diameter microlens as the electric field amplitude is increased are presented in Figure S5 (Supporting Information), where it can be seen that the behavior resembles that observed for the 255 μm diameter lenses. In addition, data for a range of droplet diameters are presented in Table S1 (Supporting Information) showing the voltage ranges for which two focal lengths are observed.

In conclusion, we have demonstrated the fabrication of electrically tunable bifocal microlenses by using drop-on-demand inkjet printing to deposit nematic LCs precisely in the 500 μm gap between in-plane electrodes. These printed droplets were found to form plano-convex lenses after impact with the substrate. A range of lens sizes were printed with a 50 μm Microfab nozzle resulting in lens diameters ranging from 120 to 255 μm , depending upon the number of drops deposited per microlens. The simple electrode arrangement on the substrate allowed us to demonstrate the electrical tunability of a printed LC microlens, which was found to exhibit a bifocal behavior due to the reorientation of the LC director in the droplet in the presence of an applied voltage. Without an applied voltage, these microlenses are found to be polarization insensitive and have an inherent focal length that ranges from 220 to 463 μm depending upon the radius of curvature of the lens. However, in the presence of a high amplitude applied voltage the focal length of the 255 μm diameter microlens is found to decrease by $140 \pm 10 \mu\text{m}$, corresponding to the larger refractive index of the LC along the director. Furthermore, it was also found that there is a range of voltages for which two focal planes are observed due to the formation of two separate domains in the LC droplet each characterized by a different refractive index profile. These findings could be of importance for 3d imaging

applications where the two separate focal planes could be used to give the impression of depth perspective.

Experimental Section

In-Plane Electrode Substrates: In-plane electrode substrates were prepared by etching an indium tin oxide-coated glass substrate using a photolithography process. This resulted in two electrodes on the surface of the glass that were separated by a gap of 500 μm . The etched substrate was then cleaned with isopropyl alcohol and rinsed with deionized water before being sonicated for 20 min in acetone. The prepared substrates were then chemically modified with a 0.02 wt% L- α -phosphatidylcholine (lecithin) solution that was spin-coated onto the substrate at 1000 rpm for 30 s and baked at 70 $^{\circ}\text{C}$ for 1 min.

Drop-on-Demand Printing: The printing setup used in this work is a commercially available printing system (Jetlab-II, Microfab Technologies Inc), which consists of four dispensers, a motorized stage and temperature-controlled print-heads and substrates. A 50 μm nozzle diameter Microfab dispenser was used to generate the LC droplets to within an accuracy of $\pm 5 \mu\text{m}$. For this study, the nematic LC, E7 (from Synthon) was used as a functional ink which has refractive indices of $n_o = 1.52$ and $n_e = 1.74$ at 633 nm and 20 $^{\circ}\text{C}$.^[29] The temperature of the print-head was set to 60 $^{\circ}\text{C}$ in order to raise the nematic LC to above its clearing temperature, $T_c = 58 \text{ }^{\circ}\text{C}$. Heating into the isotropic phase is beneficial for a stable droplet generation from the nozzle (i.e., no jet or satellite droplet formation). The pressure of the print-head was controlled using a pneumatic system to optimize the liquid flow and wetting of the nozzle-orifice. Droplet generation at the nozzle, and subsequent deposition onto the substrates, were observed using a high-speed camera (Phantom V12.1) in a shadowgraphy configuration illuminated with a halogen high-intensity white light source (OSL2 3200K, Thorlabs).

Characterization of Focal Length: To measure the focal length of the lenses, a continuous wave He–Ne laser ($\lambda = 632.8 \text{ nm}$) was used to illuminate the microlenses. A neutral density filter was used to adjust the input intensity of the laser and a half-wave plate (632.8 nm) was used to control the orientation of the input polarization. Samples were mounted on a computer-controlled linear translation stage (LNR 50S, Thorlabs) and an imaging lens of focal length 75 mm was then translated in such a way that a clear image of the focal plane of each LC lens was formed at the charge-coupled device (CCD), as shown in the bottom right of Figure 2c. The motorized stage was then translated in 5 μm steps toward the laser source. The sharpest focal spot of the LC microlens was formed as shown in the top right of Figure 2c.

Supporting Information

Supporting Information is available from the Wiley Online Library or from the author.

Acknowledgements

W.K. acknowledges the financial support provided by Punjab Education Endowment Fund (PEEF), Pakistan. The authors also gratefully acknowledge the Engineering and Physical Sciences Research Council (UK) for financial support through the project EP/R511742/1, and the John Fell Fund (Oxford University Press) through the project 0005176. W.K. would like to thank Ellis Parry and John J. Sandford O'Neill for useful discussions regarding this work.

Conflict of Interest

The authors declare no conflict of interest.

Keywords

drop-on-demand, inkjet printing, microlenses, nematic liquid crystals

Received: April 1, 2020

Revised: May 16, 2020

Published online: June 8, 2020

- [1] W. Yuan, L.-H. Li, W.-B. Lee, C.-Y. Chan, *Chin. J. Mech. Eng.* **2018**, 31, 16.
- [2] B. Aldalali, C. Li, L. Zhang, H. Jiang, *J. Microelectromech. Syst.* **2012**, 21, 945.
- [3] W. C. Sweatt, B. H. Jared, B. J. Anderson, V. Gupta, M. Okandan, G. N. Nielson, in *Renew Energy Environ. Opt. Photonics Congr.*, OSA, Washington, D.C. **2012**, p. SM2A.1.
- [4] A. Peer, R. Biswas, J.-M. Park, R. Shinar, J. Shinar, *Opt. Express* **2017**, 25, 10704.
- [5] X. Zeng, J. Plain, S. Jradi, C. Darraud, F. Louradour, R. Bachelot, P. Royer, *Opt. Express* **2011**, 19, 4805.
- [6] M.-H. Wu, C. Park, G. M. Whitesides, *Langmuir* **2002**, 18, 9312.
- [7] Y. Zhao, T. Cui, *J. Micromech. Microeng.* **2003**, 13, 430.
- [8] T. Zhou, F. Ma, B. Ruan, J. Zhou, P. Liew, X. Wang, *Int. J. Adv. Manuf. Technol.* **2019**, 103, 3003.
- [9] H. Xiong, Z. Wang, *J. Micromech. Microeng.* **2019**, 29, 085002.
- [10] T. Hou, C. Zheng, S. Bai, Q. Ma, D. Bridges, A. Hu, W. W. Duley, *Appl. Opt.* **2015**, 54, 7366.
- [11] H. Becker, C. Gärtner, *Anal. Bioanal. Chem.* **2008**, 390, 89.
- [12] Y. Luo, L. Wang, Y. Ding, H. Wei, X. Hao, D. Wang, Y. Dai, J. Shi, *Appl. Surf. Sci.* **2013**, 279, 36.
- [13] I. H. Giden, N. Eti, B. Rezaei, H. Kurt, *IEEE J. Quantum Electron.* **2016**, 52, 1.
- [14] Y. H. Lin, Y. J. Wang, V. Reshetnyak, *Liq. Cryst. Rev.* **2017**, 5, 111.
- [15] N. Chronis, G. Liu, K.-H. Jeong, L. Lee, *Opt. Express* **2003**, 11, 2370.
- [16] G. Zhu, J. Yao, S. Wu, X. Zhang, *Electrophoresis* **2019**, 40, 1148.
- [17] B. Berge, J. Peseux, *Eur. Phys. J. E* **2000**, 3, 159.
- [18] L. Dong, A. K. Agarwal, D. J. Beebe, H. Jiang, *Nature* **2006**, 442, 551.
- [19] S. Xu, Y. Li, Y. Liu, J. Sun, H. Ren, S.-T. Wu, *Micromachines* **2014**, 5, 300.
- [20] H.-C. Lin, M.-S. Chen, Y.-H. Lin, *Trans. Electr. Electron. Mater.* **2011**, 12, 234.
- [21] C. Y. Chien, C. H. Li, C. R. Sheu, *Crystals* **2017**, 7, 209.
- [22] E. Parry, S. Bolis, S. J. Elston, A. A. Castrejón-Pita, S. M. Morris, *Adv. Eng. Mater.* **2018**, 20, 1700774.
- [23] J. F. Algorri, V. Urruchi del Pozo, J. M. Sanchez-Pena, J. M. Oton, *J. Disp. Technol.* **2014**, 10, 713.
- [24] J.-H. Han, J. Moon, D.-H. Cho, J.-W. Shin, H. Y. Chu, J.-I. Lee, N. S. Cho, J. Lee, *J. Inf. Disp.* **2018**, 19, 179.
- [25] K. Li, A. Ö. Yöntem, Y. Deng, P. Shrestha, D. Chu, J. Zhou, J. Yao, *Opt. Express* **2017**, 25, 9654.
- [26] P. G. de Gennes, *Rev. Mod. Phys.* **1985**, 57, 827.
- [27] S.-U. Kim, S. Lee, J.-H. Na, S.-D. Lee, *Opt. Commun.* **2014**, 313, 329.
- [28] H. Ren, Y.-H. Fan, S.-T. Wu, *Opt. Lett.* **2004**, 29, 1608.
- [29] J. Li, G. Baird, Y.-H. Lin, H. Ren, S.-T. Wu, *J. Soc. Inf. Disp.* **2005**, 13, 1017.